



# Aeroservoelastic design of piezo-composite wings for gust load alleviation

Haojie Liu, Xiao Wang\*

State Key Laboratory of Mechanics and Control of Mechanical Structures, State Key Laboratory of Rotorcraft Aeromechanics, College of Aerospace Engineering, Nanjing University of Aeronautics and Astronautics, China



## ARTICLE INFO

### Article history:

Received 26 November 2018

Received in revised form 29 March 2019

Accepted 19 April 2019

Available online 10 May 2019

### Keywords:

Thin-walled beam

Piezo-composite wing

Gust load alleviation

Piezo-actuator

Fiber-reinforced

## ABSTRACT

In this study, aeroservoelastic design of piezo-composite wings is performed to minimize gust responses. The wing structure is modeled as a composite thin-walled beam featuring fiber-reinforced host structure and piezo-actuators whose anisotropic characteristics are accounted. In addition, doublet-lattice method and rational function approximation technique are integrated to establish the aeroservoelastic model. State feedback H-infinity controllers are synthesized for different wing configurations in order to assess the closed-loop effectiveness. Numerical results demonstrate that the gust load alleviation performance is sensitive to the piezo-actuator ply-angle, namely of that the gust response can be effectively suppressed for the wing configuration with appropriate ply-angle.

© 2019 Elsevier Ltd. All rights reserved.

## 1. Introduction

Nowadays, composite materials have been widely used in aerospace engineering due to light weight, high strength and stiffness. In addition to the aforementioned advantages, the unique directionality properties of composite materials can be exploited for aeroelastic tailoring, a passive control technique to improve aeroelastic performance. Previous studies have demonstrated that desirable aeroelastic behaviors can be achieved by altering the structure directional stiffness (Shirk et al., 1986; Jutte and Stanford, 2014; Guo, 2007; Kameyama and Fukunaga, 2007; Weisshaar and Duke, 2006; Librescu and Khdeir, 1988; Lottati, 1985; Pettit and Grandhi, 2003; Kim and Hwang, 2005). In general, the applications of composite materials for aeroelastic tailoring include weight reduction (Guo, 2007; Kameyama and Fukunaga, 2007), drag reduction (Weisshaar and Duke, 2006), flutter and divergence speed maximization (Librescu and Khdeir, 1988; Lottati, 1985), and gust load alleviation (Pettit and Grandhi, 2003; Kim and Hwang, 2005). In addition to passive aeroelastic control, recent years have witnessed a series of studies on active aeroelastic control that expands the traditional flutter boundaries (Livre, 2017; Mukhopadhyay, 2000; Behal et al., 2006; Zhang and Singh, 2001; Huang et al., 2012a,b, 2015, 2016; Liu et al., 2016) and improves ride qualities (Zeng et al., 2012; Zhao et al., 2016; Haghigat et al., 2012; Fonte et al., 2015). In these researches, control surfaces including spoilers and ailerons are actively controlled to modify the aerodynamic shape. Active aeroelastic control technologies based on control surfaces, although widely studied, have several limitations such as large number of parts and multiple energy conversions (Giurgiutiu, 2000). With the developments of smart or intelligent materials, many researches of active aeroelastic control have been conducted based on piezoelectric, shape memory alloy and other smart materials recently (Suleman and Costa, 2004; Han et al., 2006; Heinze and Karpel, 2006; Bae et al., 2005; Barzegari et al., 2015; Candido de Sousa and De Marqui Jr., 2018; Wang et al.,

\* Corresponding author.

E-mail address: [x.wang@nuaa.edu.cn](mailto:x.wang@nuaa.edu.cn) (X. Wang).

## Nomenclature

$u_0, v_0, w_0$	Translation of the cross-section about three axis $x, y, z$
$\theta_x, \phi, \theta_z$	Rotation of the cross-section about three axis $x, y, z$
$\theta_h, \theta_p$	Ply-angles in host structure and piezo-actuator
$h$	Wall thickness
$\dot{\zeta}, \ddot{\zeta}, \zeta'$	$\partial\zeta/\partial t, \partial^2\zeta/\partial t^2, \partial\zeta/\partial y$
$F_w(q), a(q)$	Primary and secondary warping functions
$\psi(q)$	Torsional function
$\varepsilon_{yy}, \gamma_{yy}$	Spanwise and transverse shear strain
$\oint_c, \int_0^L$	Integral along the cross-section and the span, respectively
$m_l$	Total number of the constituent layers
$T, U$	Kinetic energy and strain energy
$\rho(k)$	Mass density of the $k$ th layer
$b_{ij}$	Inertial coefficients
$M_x, M_y, B_w$	Bending moment, torque and bimoment
$Q_z$	Transverse shear force
$\delta$	Variation operator
$a_{ij}$	1-D global stiffness coefficients
$R(y)$	Actuator span location
$\aleph_1^{M_x}, \aleph_1^{M_y}, \aleph_2^{Q_z}, \aleph_1^{B_w}$	Piezo-coefficients
$\delta_p, \delta_s$	Tracers that take the value 1 or 0
$V_p$	Voltage input
$\mathbf{M}, \mathbf{D}, \mathbf{K}$	Generalized mass, damping and stiffness matrices
$\mathbf{f}_p$	Generalized force vector related with unit voltage input
$\mathbf{q}$	Generalized displacement vector
$\mathbf{Q}_q, \mathbf{Q}_g$	Generalized aerodynamic force coefficient matrices
$s$	Laplace variable
$w_g$	Velocity of the atmosphere gust
$a$	Parameter of low-pass filter for Dryden model
$\rho_\infty$	Free-stream density
$V_\infty, M_\infty$	Free-stream velocity and Mach number
$q_\infty$	dynamic pressure
$k_R$	Reduced frequency
$b_R$	Reference length
$\mathbf{x}_a$	Aerodynamic state vector
$\mathbf{f}_a$	Generalized aerodynamic force vector
$\Phi_w(\omega)$	Power spectral density function of Dryden model
$\sigma_w, L_w$	RMS value and the scale of the continuous gust
$r$	White-noise signal with $\Phi_r(\omega) = 1$
$\mathbf{x}_g$	State vector of Dryden model
$M_r$	Wing-root bending moment
$\eta$	Weight parameter

2018; Na and Librescu, 1998; Librescu et al., 2008; Na et al., 2011). Among these smart materials, piezoelectric materials have drawn many attentions due to a lot of desirable characteristics, such as fast response, high control bandwidth and mechanical simplicity. However, most of previous researches assume that the materials of the piezoelectric actuators are isotropic. The consequence of such assumption is that active control systems are synthesized with piezoelectric bending moment control effects and with piezoelectric torque control effects neglected. Wang et al. (2017b,a) developed a composite thin-walled beam theory with anisotropy piezo-composite. Based on the semi-analytic solution of the adaptive beam model, comprehensive discussions on coupling of piezoelectrically induced extension, transverse shear, twist, warping and bending actuations were addressed.

In this study, based on the structural model developed by Wang et al. (2017b), aeroservoelastic design is further performed in order to identify the optimal wing configuration that minimizes gust responses. The wing structure is modeled as a composite thin-walled beam featuring fiber-reinforced host structure and piezo-actuators whose anisotropic

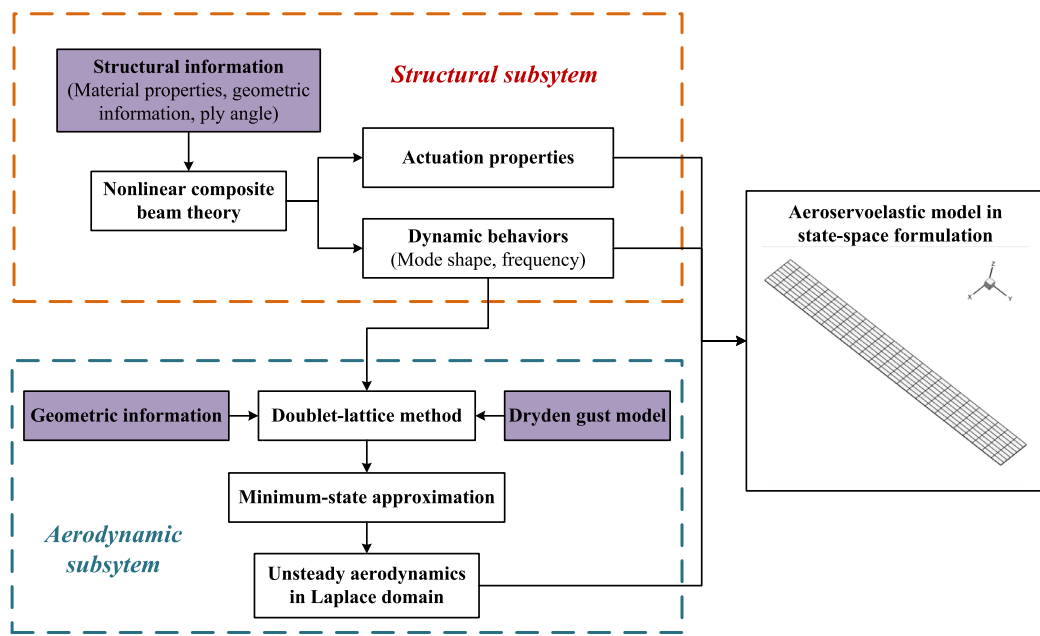


**Fig. 1.** Aeroservoelastic modeling procedure for a piezo-composite wing.

characteristics are accounted. Furthermore, it is assumed that the piezo-actuators are embedded in the host structure by Circumferentially Asymmetric Stiffness (CAS) configuration. Therefore, the wing structure can be controlled by a coupled piezoelectric torque-bending moment actuation. Considering facts that on one hand various design parameters have significant effects on control performance, on the other hand different performance indicators of the aeroservoelastic system will be defined to fulfill the requirements for various flight conditions, it is an extremely difficult task to implement a comprehensive investigation. Thus, in the present article, we will focus on the wing configuration with the maximum instability speed and investigate the effects of piezo-actuator ply-angles on the gust load alleviation performance.

The remainder of this study is organized as follows. In Section 2, the numerical modeling procedure to establish the aeroservoelastic model of a piezo-composite wing is described. In Section 3, the host structure of a wing configuration with the maximum instability speed is determined at first. State feedback H-infinity controllers are synthesized for different piezo-actuator ply-angles and the gust load alleviation performance is investigated. Finally, some conclusions are drawn in Section 4.

## 2. Aeroservoelastic modeling of smart piezo-composite wings

In this section, the aeroservoelastic model in state-space form is developed for a piezo-composite wing by integrating refined thin-walled beam theory with piezo-composite materials, doublet-lattice method and rational function approximation technique. At first, the dynamic and actuation behaviors of the piezo-composite wing are obtained via a composite thin-walled beam theory. Subsequently, the doublet-lattice method is implemented to model the unsteady aerodynamic loads in frequency domain. Then, the minimum-state approximation is applied to transform the unsteady aerodynamics from frequency domain to Laplace domain. In the end, the aeroservoelastic model in state-space form can be established for the piezo-composite wing by integrating the aforementioned subsystems. The flowchart of the aeroservoelastic modeling procedure is presented in Fig. 1.

### 2.1. Structural model

A single-cell, closed cross-section, thin-walled beam model incorporating fiber-reinforced and piezoelectric composite materials is used in the modeling of piezo-composite wings and toward the study of active aeroelastic control. Fig. 2 presents the geometry of a piezo-composite wing.

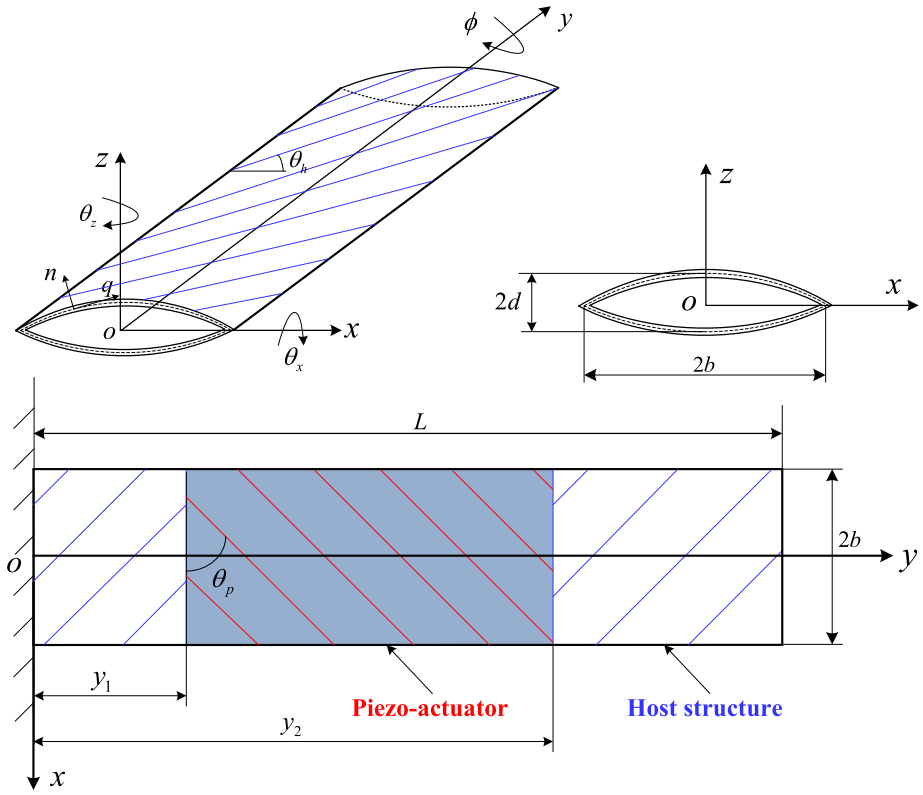


**Fig. 2.** Piezo-composite wing modeled as a thin-walled beam.

Based on the assumptions stipulated in Refs. Qin and Librescu (2002) and Wang and Qin (2016), the following representation of the three dimensional displacements is postulated

$$\begin{aligned} u(x, y, z, t) &= u_0(y, t) + z\phi(y, t) \\ v(x, y, z, t) &= v_0(y, t) + \left[ x(q) - n\frac{dz}{dq} \right] \theta_z(y, t) + \left[ z(q) + n\frac{dx}{dq} \right] \theta_x(y, t) \\ &\quad - [F_w(q) + na(q)]\phi'(y, t) \\ w(x, y, z, t) &= w_0(y, t) - x\phi(y, t) \end{aligned} \quad (1)$$

where  $F_w(q)$  and  $a(q)$  are the primary and secondary warping functions, respectively. The terms  $u_0, v_0, w_0$  and  $\theta_x, \phi, \theta_z$  are the associated translation and rotation displacement components of the cross-section about three axis ( $x, y, z$  direction), respectively. These six kinematic variables, which represent one dimensional displacement measures, constitute the basic unknowns of the structural model. The nonzero strains contributing to the potential are given as follows.

Spanwise strain:

$$\varepsilon_{yy}(n, q, y, t) = \varepsilon_{yy}^0(q, y, t) + n\varepsilon_{yy}^1(q, y, t) \quad (2)$$

where the axial strain components  $\varepsilon_{yy}^0$  and  $\varepsilon_{yy}^1$  are associated with the primary and secondary warping, respectively, i.e.,

$$\begin{aligned} \varepsilon_{yy}^0(q, y, t) &= v_0'(y, t) + \theta_z'(y, t)x(y, t) - F_w(q)\phi''(y, t) \\ \varepsilon_{yy}^1(q, y, t) &= \theta_x'(y, t)\frac{dx}{dq} - \theta_z'(y, t)\frac{dz}{dq} - a(q)\phi''(y, t) \end{aligned} \quad (3)$$

Tangential shear strain:

$$\gamma_{sy}(q, y, t) = [u_0'(y, t) + \theta_z(y, t)]\frac{dx}{dq} + [w_0'(y, t) + \theta_x(y, t)]\frac{dz}{dq} + \psi(q)\phi'(y, t) \quad (4)$$

where the torsional function  $\psi(q)$  is defined in Ref. Qin and Librescu (2002).

Transverse shear strain:

$$\gamma_{ny}(q, y, t) = [w_0'(y, t) + \theta_x(y, t)] \frac{dx}{dq} - [u_0'(y, t) + \theta_z(y, t)] \frac{dz}{dq} \quad (5)$$

We assume that both the fiber-reinforced composite material of the host structure and the piezo-composite material of the piezo-actuator can be modeled with a linear piezoelectric constitutive relationship (Yang, 2004; Fang and Liu, 2013). The structural governing equations and the associated boundary conditions are derived from Hamilton's principle. This principle states that the true path of motion renders the following variational form stationary

$$\delta J = \int_{t_1}^{t_2} (\delta T - \delta U) dt = 0 \quad (6)$$

where  $t_1$  and  $t_2$  denote two arbitrary motions of time. The kinetic energy  $T$  and the strain energy  $U$  are defined as

$$\begin{aligned} T &= \frac{1}{2} \int_0^L \oint_c \sum_{k=1}^{m_l} \int_{h(k)} \rho_{(k)} \left[ \left( \frac{\partial u}{\partial t} \right)^2 + \left( \frac{\partial v}{\partial t} \right)^2 + \left( \frac{\partial w}{\partial t} \right)^2 \right] dndqdy \\ U &= \frac{1}{2} \int_0^L \oint_c \sum_{k=1}^{N_{hp}} [\sigma_{yy}\varepsilon_{yy} + \sigma_{yq}\gamma_{qy} + \sigma_{ny}\gamma_{ny}]_{h(k)} dqdy \end{aligned} \quad (7)$$

In order to study the aeroelastic problems featuring bending-twist elastic coupling that is beneficial for the aeroelastic response behavior (Librescu and Khdeir, 1988; Librescu et al., 2008), a beam configured by the CAS lay-up (both for host structure and piezo-actuator parts) and characterized by a biconvex cross-section is considered. As demonstrated in Refs. Librescu and Song (1991) and Librescu et al. (1996), the elastic coupling of this type of beams can be split into two independent groups, viz., flapwise bending-twist-flapwise transverse shear and chordwise bending-extension-chordwise transverse shear elastic couplings. Thus, after a lengthy variation process of Eq. (6) and collecting the terms associated with the same variations, the governing equations of the bending-twist subsystem that are of interest for the present problem are

$$\begin{aligned} \delta w_0: \bar{Q}_z' + \tilde{Q}_z' - b_1 \ddot{w}_0 &= 0 \\ \delta \phi: \bar{M}_y' + \tilde{M}_y' - \bar{B}_w'' - \tilde{B}_w'' - (b_4 + b_5) \ddot{\phi} + (b_{10} + b_{18}) \ddot{\phi}'' &= 0 \\ \delta \theta_x: \bar{M}_x' + \tilde{M}_x' - \bar{Q}_z - \tilde{Q}_z - (b_4 + b_{14}) \ddot{\theta}_x &= 0 \end{aligned} \quad (8)$$

The associated boundary conditions at the beam root are

$$w_0(0) = \phi(0) = \phi'(0) = \theta_x(0) = 0 \quad (9)$$

and at the beam tip are

$$\begin{aligned} \delta w_0: \bar{Q}_z(L) + \tilde{Q}_z(L) &= 0 \\ \delta \phi: \bar{M}_y(L) + \tilde{M}_y(L) - \bar{B}_w'(L) - \tilde{B}_w'(L) + (b_{10} + b_{18}) \ddot{\phi}'(L) &= 0 \\ \delta \phi': \bar{B}_w(L) + \tilde{B}_w(L) &= 0 \\ \delta \theta_x: \bar{M}_x(L) + \tilde{M}_x(L) &= 0 \end{aligned} \quad (10)$$

In the above equations, the inertial coefficients  $b_{ij}$  are defined in the appendix of Ref. Wang and Qin (2016); flapwise bending moment  $M_x$ , flapwise transverse shear force  $Q_z$ , torque  $M_y$  and bimoment  $B_w$ , with over-bar ( $\bar{\bullet}$ ) and over-tilde ( $\tilde{\bullet}$ ) identify the pure mechanical and piezo-actuator measures contributions, respectively.

For biconvex cross-section thin-walled beams with CAS lay-up configuration, the mechanical force-displacement relations can be simplified as (Qin and Librescu, 2003)

$$\begin{Bmatrix} \bar{M}_x \\ \bar{M}_y \end{Bmatrix} = \begin{bmatrix} a_{33} & a_{37} \\ a_{37} & a_{77} \end{bmatrix} \begin{Bmatrix} \theta_x' \\ \phi' \end{Bmatrix}, \quad \begin{Bmatrix} \bar{Q}_z \\ \bar{B}_w \end{Bmatrix} = \begin{bmatrix} a_{55} & a_{56} \\ a_{56} & a_{66} \end{bmatrix} \begin{Bmatrix} \theta_x + w_0' \\ \phi'' \end{Bmatrix} \quad (11)$$

where the stiffness coefficients  $a_{ij}$  are defined in the appendix of Ref. Wang and Qin (2016). When the piezo-composite layers embedded in the biconvex cross-section beams is configured by CAS lay-up, the relation between piezoelectrically induced actuators and applied voltages can be simplified as

$$\begin{aligned} \begin{Bmatrix} \tilde{M}_x(y, t) \\ \tilde{M}_y(y, t) \end{Bmatrix} &= \begin{Bmatrix} \mathbf{x}_1^{M_x} \\ \mathbf{x}_1^{M_y} \end{Bmatrix} V_p(t) R(y), \quad \begin{Bmatrix} \tilde{Q}_z(y, t) \\ \tilde{B}_w(y, t) \end{Bmatrix} = \begin{Bmatrix} \mathbf{x}_2^{Q_z} \\ \mathbf{x}_1^{B_w} \end{Bmatrix} V_q(t) R(y) \\ V_p(t) &= \frac{1}{2} [V_T(t) - V_B(t)], \quad V_q(t) = \frac{1}{2} [V_T(t) + V_B(t)] \end{aligned} \quad (12)$$

where  $V_T$  and  $V_B$  denote the voltages on the piezo-actuators located on the top and bottom of the wall; definitions of piezo-coefficients  $\aleph_1^{M_x}$ ,  $\aleph_1^{M_y}$ ,  $\aleph_2^{Q_z}$  and  $\aleph_1^{B_w}$  are given in the appendix of Ref. Wang et al. (2017b).  $R(y)$  of Eq. (12) denotes the piezo-actuator location along span. It needs to be noted that the effect of the piezoelectrically induced flapwise transverse shear force  $\tilde{Q}_z$  and bimoment  $\tilde{B}_w$  on control authority are both immaterial (Wang et al., 2017b). Therefore, they can be eliminated in the governing equations safely, resulting that the system is solely controlled by the voltage parameter  $V_p$ . By substituting Eqs. (11) and (12) into Eqs. (8)–(10), the governing equations expressed in terms of the basic unknowns are

$$\begin{aligned} \delta w_0: & a_{55}(w_0'' + \theta_x') + a_{56}\phi''' - b_1\ddot{w}_0 = 0 \\ \delta\phi: & a_{37}\theta_x'' + a_{77}\phi'' - a_{66}\phi^{(iv)} - a_{56}(w_0'' + \theta_x'') - (b_4 + b_5)\ddot{\phi} \\ & + (b_{10} + b_{18})\ddot{\phi}'' + \delta_p\aleph_1^{M_y}V_pR'(y) = 0 \\ \delta\theta_x: & a_{33}\theta_x'' + a_{37}\phi'' - a_{55}(w_0' + \theta_x) - a_{56}\phi'' - (b_4 + b_{14})\ddot{\theta}_x \\ & + \delta_p\aleph_1^{M_x}V_pR'(y) = 0 \end{aligned} \quad (13)$$

The boundary conditions are  
at  $y = 0$ :

$$w_0 = \phi = \phi' = \theta_x = 0 \quad (14)$$

and at  $y = L$ :

$$\begin{aligned} \delta w_0: & a_{55}(w_0' + \theta_x) + a_{56}\phi'' = 0 \\ \delta\phi: & a_{37}\theta_x' + a_{77}\phi' - a_{66}\phi''' - a_{56}(w_0'' + \theta_x') + (b_{10} + b_{18})\ddot{\phi}'' + \delta_s\aleph_1^{M_y}V_p = 0 \\ \delta\phi': & a_{56}(w_0' + \theta_x) + a_{66}\phi'' = 0 \\ \delta\theta_x: & a_{33}\theta_x' + a_{37}\phi' + \delta_s\aleph_1^{M_x}V_p = 0 \end{aligned} \quad (15)$$

Note that the traces  $\delta_p = 0$  and  $\delta_s = 1$  for the case the actuator is spread over the entire beam span, otherwise their values are assumed as  $\delta_p = 1$  and  $\delta_s = 0$ .

The Extended Galerkin's Method (Librescu et al., 1997) is used to semi-discretize the system for numerical study. We assume

$$u_0 = \Psi_u^T(y)\mathbf{q}_u(t), \quad w_0 = \Psi_w^T(y)\mathbf{q}_w(t), \quad \theta_x = \Psi_x^T(y)\mathbf{q}_x(t), \quad \theta_z = \Psi_z^T(y)\mathbf{q}_z(t) \quad (16)$$

Thus, the structural model of the smart piezo-composite wing in modal space can be obtained as follows

$$\mathbf{M}\ddot{\mathbf{q}} + \mathbf{D}\dot{\mathbf{q}} + \mathbf{K}\mathbf{q} = \mathbf{f}_p V_p \quad (17)$$

where  $\mathbf{q}$  is the generalized displacement vector as

$$\mathbf{q} = [\mathbf{q}_u \quad \mathbf{q}_w \quad \mathbf{q}_x \quad \mathbf{q}_z]^T \quad (18)$$

$\mathbf{M}$ ,  $\mathbf{D}$  and  $\mathbf{K}$  are the generalized mass, damping and stiffness matrices, respectively.  $\mathbf{f}_p$  represents the generalized force vector related with unit voltage input  $V_p$ . Their explicit expressions are given in the appendix of Ref. Wang et al. (2017b).

## 2.2. Aerodynamic model

The generalized aerodynamic forces exerted on a piezo-composite wing can be obtained via doublet-lattice method as

$$\mathbf{f}_a(k_R, M_\infty) = q_\infty \mathbf{Q}_q(k_R, M_\infty) \mathbf{q}(s) + q_\infty \mathbf{Q}_g(k_R, M_\infty) \frac{w_g(s)}{V_\infty} \quad (19)$$

where  $s$  is Laplace variable and  $w_g$  is the velocity of the atmosphere gust.  $V_\infty$  is the free-stream velocity and  $q_\infty$  represents the dynamic pressure.  $\mathbf{Q}_q$  and  $\mathbf{Q}_g$  are the generalized aerodynamic force coefficient matrices which are functions of reduced frequency  $k_R$  and free-stream Mach number  $M_\infty$ .

In order to cast the aerodynamic model in Eq. (19) into state-space form, the matrices  $\mathbf{Q}_q$  and  $\mathbf{Q}_g$  in frequency domain need to be transformed to Laplace domain via rational function approximation techniques. In the present study, the minimum-state approximation technique (Karpel et al., 2004) is implemented for such purpose and  $\mathbf{Q}_q$  and  $\mathbf{Q}_g$  can be approximated as

$$\begin{aligned} [\mathbf{Q}_q \mathbf{Q}_g] = & [\mathbf{A}_{q0} \mathbf{A}_{g0}] + [\mathbf{A}_{q1} \mathbf{A}_{g1}] ik_R + [\mathbf{A}_{q2} \mathbf{0}] (ik_R)^2 \\ & + D_w (ik_R \mathbf{I} - \mathbf{R}_w)^{-1} [\mathbf{E}_q \mathbf{E}_g] ik_R \end{aligned} \quad (20)$$

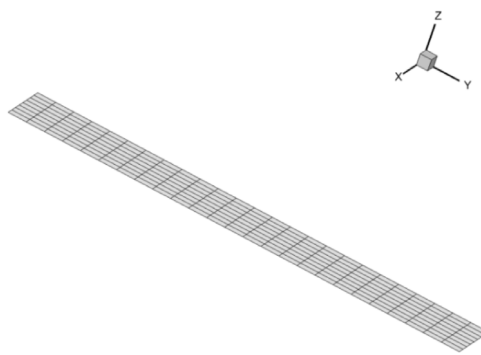


**Fig. 3.** Aerodynamic grid for flutter prediction.

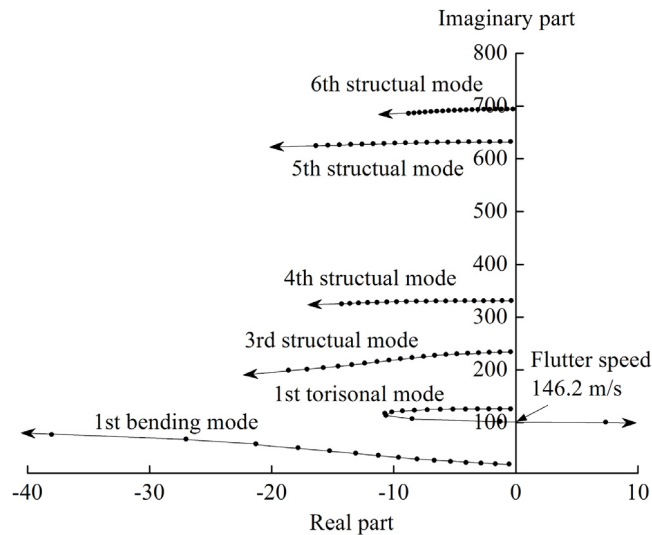


**Fig. 4.** Root-locus diagram of the composite wing.

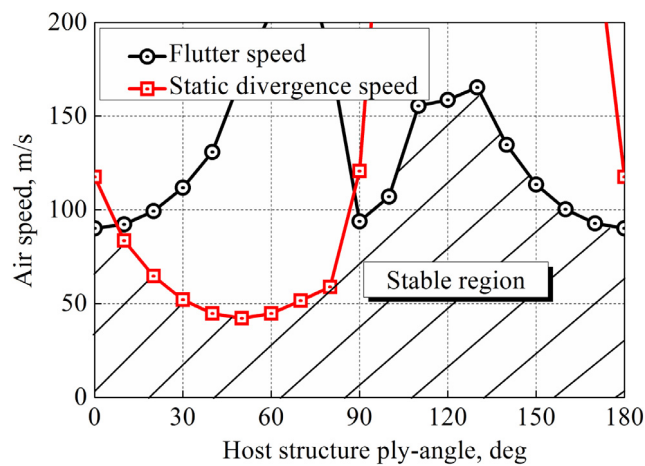


**Fig. 5.** Instability boundaries of the piezo-composite wing.

**Table 1**  
Geometric information of the piezo-composite wing.

Parameter	Value
Width $2b$	0.757 m
Depth $2d$	0.1 m
Wall thickness $h$	0.03 m
Length $L$	6.058 m
Number of layers $m_h$	6

**Table 2**  
Material properties of the piezo-composite wing.

Parameter	Host structure	Piezo-actuator
$E_{11}$	$206.8 \times 10^9 \text{ N m}^{-2}$	$31.28 \times 10^9 \text{ N m}^{-2}$
$E_{22} = E_{33}$	$5.17 \times 10^9 \text{ N m}^{-2}$	$17.05 \times 10^9 \text{ N m}^{-2}$
$G_{13} = G_{23}$	$2.55 \times 10^9 \text{ N m}^{-2}$	$5.12 \times 10^9 \text{ N m}^{-2}$
$G_{12}$	$3.10 \times 10^9 \text{ N m}^{-2}$	$5.12 \times 10^9 \text{ N m}^{-2}$
$\mu_{12} = \mu_{13} = \mu_{23}$	0.25	0.303
$\rho$	$1528.0 \text{ kg m}^{-3}$	$5115.9 \text{ kg m}^{-3}$
$d_{11}$	/	$386.63 \times 10^{-12} \text{ m V}^{-1}$
$d_{12} = d_{13}$	/	$-175.50 \times 10^{-12} \text{ m V}^{-1}$
Thickness of layer	5 mm	0.4318 mm
Electrode spacing	/	0.1905 m

**Table 3**  
Three flight conditions: Case 1–3.

Flight conditions	Flight parameters			
	$V_\infty$ (m/s)	$\rho_\infty$ (kg/m <sup>3</sup> )	$L_w$ (m)	$\sigma_w$ (m/s)
Case 1	100.0	1.225	200.0	2.0
Case 2	100.0	1.225	200.0	1.0
Case 3	50.0	1.225	100.0	1.0

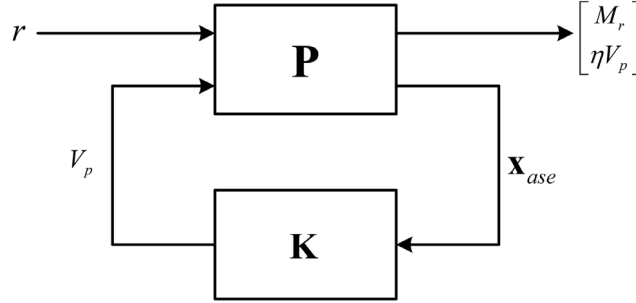


**Fig. 6.**  $H_\infty$  control diagram for gust load alleviation.

By substituting  $ik_R = \frac{i\omega b_R}{V_\infty} \Rightarrow \frac{b_R s}{V_\infty}$  where  $b_R$  is the reference length into Eq. (20), the aerodynamic matrices in Laplace domain can be obtained as

$$\begin{aligned} [\mathbf{Q}_q(s) \ \mathbf{Q}_g(s)] &= [\mathbf{A}_{q0} \mathbf{A}_{g0}] + [\mathbf{A}_{q1} \mathbf{A}_{g1}] \frac{b_R s}{V_\infty} + [\mathbf{A}_{q2} \mathbf{0}] \left( \frac{b_R s}{V_\infty} \right)^2 \\ &\quad + D_w \left( s\mathbf{I} - \frac{V_\infty}{b_R} \mathbf{R}_w \right)^{-1} [\mathbf{E}_q \ \mathbf{E}_g] s \end{aligned} \quad (21)$$

In order to facilitate the state-space formulations, the following additional aerodynamic state vector  $\mathbf{x}_a$  is defined as

$$\mathbf{x}_a(s) = \left( s\mathbf{I} - \frac{V_\infty}{b_R} \mathbf{R}_w \right)^{-1} [\mathbf{E}_q \ \mathbf{E}_g] s \begin{bmatrix} \mathbf{q}(s) \\ w_g(s)/V_\infty \end{bmatrix} \quad (22)$$

**Table 4**  
Weighting parameters for different piezo-composite wings.

Piezo-actuator ply-angle $\theta_p$ (deg)	Weighting parameter $\eta$		
	Case 1	Case 2	Case 3
0	1.30	0.90	0.90
5	1.24	0.86	0.83
10	1.15	0.80	0.73
15	1.02	0.72	0.58
20	0.85	0.59	0.36
25	0.54	0.34	0.58
30	0.84	0.56	0.84
35	1.21	0.84	1.05
40	1.55	1.05	1.22
45	1.84	1.23	1.34
50	2.10	1.36	1.44
55	2.29	1.46	1.47
60	2.45	1.52	1.49
65	2.57	1.55	1.47
70	2.65	1.57	1.47
75	2.69	1.57	1.44
80	2.75	1.57	1.46
85	2.73	1.59	1.45
90	2.71	1.59	1.47
95	2.68	1.60	1.49
100	2.63	1.59	1.49
105	2.55	1.58	1.48
110	2.44	1.55	1.45
115	2.29	1.48	1.36
120	2.08	1.39	1.23
125	1.82	1.25	1.03
130	1.51	1.04	0.75
135	1.12	0.76	0.44
140	0.58	0.36	0.75
145	0.90	0.60	0.91
150	1.13	0.78	0.99
155	1.27	0.87	1.03
160	1.33	0.92	1.03
165	1.36	0.94	1.02
170	1.35	0.94	1.00
175	1.33	0.92	0.96
180	1.30	0.90	0.90

Therefore, the generalized aerodynamic forces associated with structural displacements and gust excitations can be written in time domain as

$$\mathbf{f}_a = q_\infty \left( \mathbf{A}_{q0} \mathbf{q} + \frac{b_R}{V_\infty} \mathbf{A}_{q1} \dot{\mathbf{q}} + \left( \frac{b_R}{V_\infty} \right)^2 \mathbf{A}_{q2} \ddot{\mathbf{q}} \right) + q_\infty \left( \mathbf{A}_{g0} \frac{w_g}{V_\infty} + \frac{b_R}{V_\infty} \mathbf{A}_{g1} \frac{\dot{w}_g}{V_\infty} \right) + q_\infty \mathbf{D}_w \mathbf{x}_a \quad (23)$$

### 2.3. Aeroviscoelastic model

The aeroviscoelastic model of the smart piezo-composite wing can be obtained by integrating the aforementioned structural model and aerodynamic model as follows

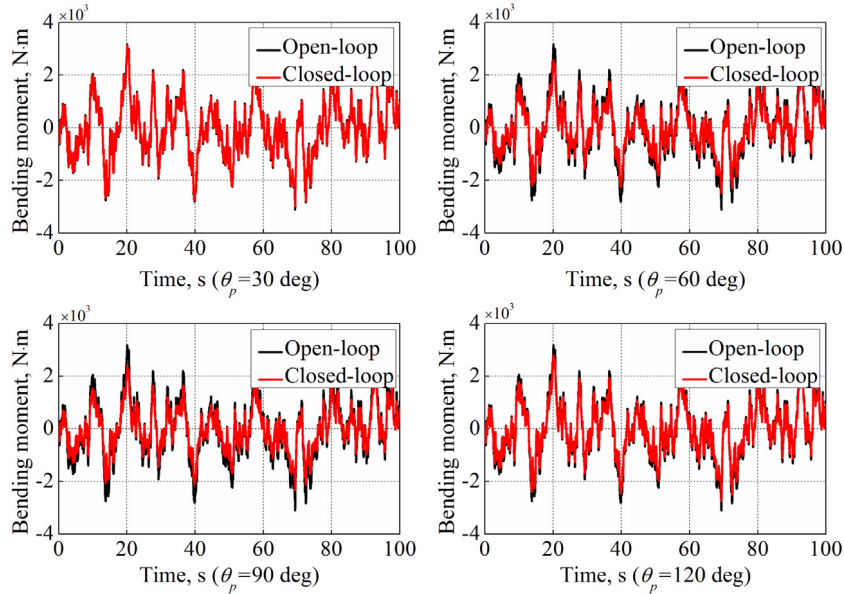
$$\begin{aligned} \mathbf{M} \ddot{\mathbf{q}} + \mathbf{D} \dot{\mathbf{q}} + \mathbf{K} \mathbf{q} &= \mathbf{f}_p V_p + q_\infty \left( \mathbf{A}_{q0} \mathbf{q} + \frac{b_R}{V_\infty} \mathbf{A}_{q1} \dot{\mathbf{q}} + \left( \frac{b_R}{V_\infty} \right)^2 \mathbf{A}_{q2} \ddot{\mathbf{q}} \right) \\ &\quad + q_\infty \left( \mathbf{A}_{g0} \frac{w_g}{V_\infty} + \frac{b_R}{V_\infty} \mathbf{A}_{g1} \frac{\dot{w}_g}{V_\infty} \right) + q_\infty \mathbf{D}_w \mathbf{x}_a \\ \dot{\mathbf{x}}_a &= \frac{V_\infty}{b_R} \mathbf{R}_w \mathbf{x}_a + \mathbf{E}_q \dot{\mathbf{q}} + \mathbf{E}_g \frac{\dot{w}_g}{V_\infty} \end{aligned} \quad (24)$$

The state-space formulation of the open-loop aeroviscoelastic equation can be obtained as

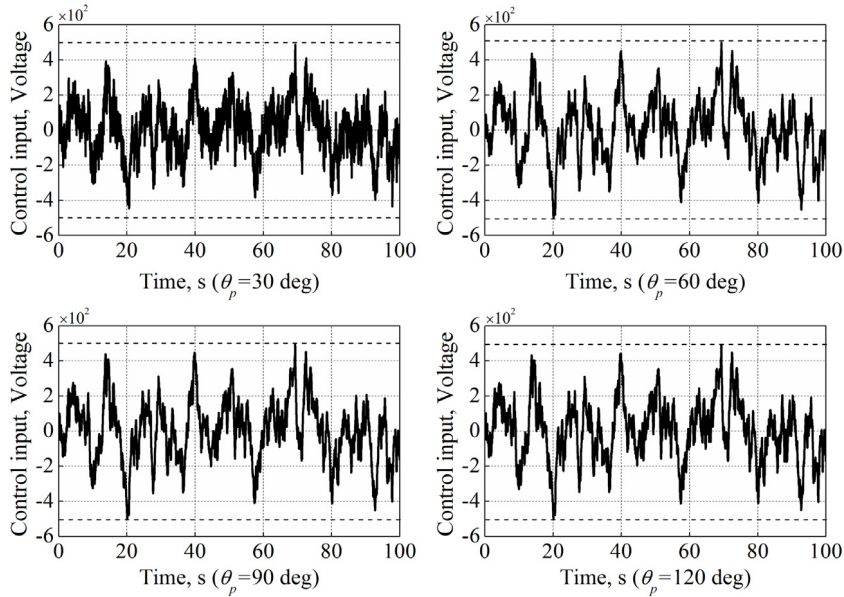
$$\dot{\mathbf{x}}_{ae} = \mathbf{A}_{ae} \mathbf{x}_{ae} + \mathbf{b}_p V_p + \mathbf{B}_{aw} \widetilde{\mathbf{w}}_g \quad (25)$$

where

$$\mathbf{x}_{ae} = [\mathbf{q} \ \dot{\mathbf{q}} \ \mathbf{x}_a]^T, \ \widetilde{\mathbf{w}}_g = [w_g \ \dot{w}_g]^T \quad (26)$$



a) Time responses of the wing-root bending moment



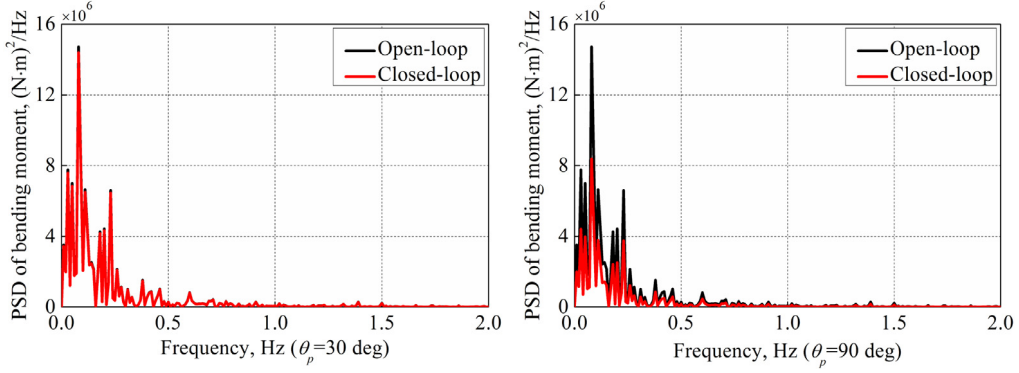
b) Time responses of control input

Fig. 7. Dynamic responses of piezo-composite wings for case 1.

For the readability, the information of the matrices  $\mathbf{A}_{ae}$ ,  $\mathbf{b}_p$  and  $\mathbf{B}_{aw}$  is given in the [Appendix](#).

In this study, the Dryden model is applied for a continuous gust, the power spectral density function of which is given by

$$\phi_w(\omega) = \sigma_w^2 \frac{\tau_w}{\pi} \frac{1 + 3(\omega\tau_w)}{\left[1 + (\omega\tau_w)^2\right]^2} \quad (27)$$



**Fig. 8.** PSD curves of the wing-root bending moment for case 1.

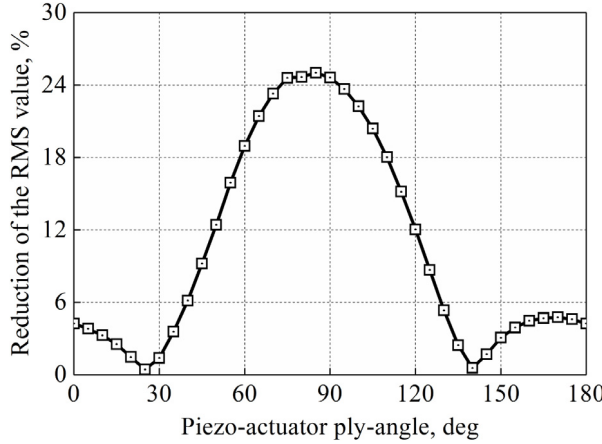


**Fig. 9.** Load alleviation performance of different piezo-composite wings for case 1.

where  $\tau_w = L_w/V_\infty$ . The terms  $\sigma_w$  and  $L_w$  represent the Root-Mean-Square (RMS) value and the scale of the continuous gust, respectively. The gust can be obtained by defining a gust filter that is excited by white noise

$$\frac{w_g(s)}{r(s)} = \sigma_w \frac{1}{\sqrt{\pi}} \frac{\sqrt{3}\tau_w^{-1/2}s + \tau_w^{-3/2}}{(s + 1/\tau_w)^2} \frac{a}{s + a} \quad (28)$$

where  $r(s)$  represents the white-noise signal with power spectral density function  $\Phi_r(\omega) = 1$ . In Eq. (28),  $a/(s + a)$  represents a low-pass filter used to avoid the occurrence of non-converged RMS acceleration response. By defining state vector  $\mathbf{x}_g = [x_g \dot{x}_g \ddot{x}_g]^T$  and  $\tilde{\mathbf{w}}_g = [w_g \dot{w}_g]^T$ , the state-space formulation of the Dryden model can be obtained as

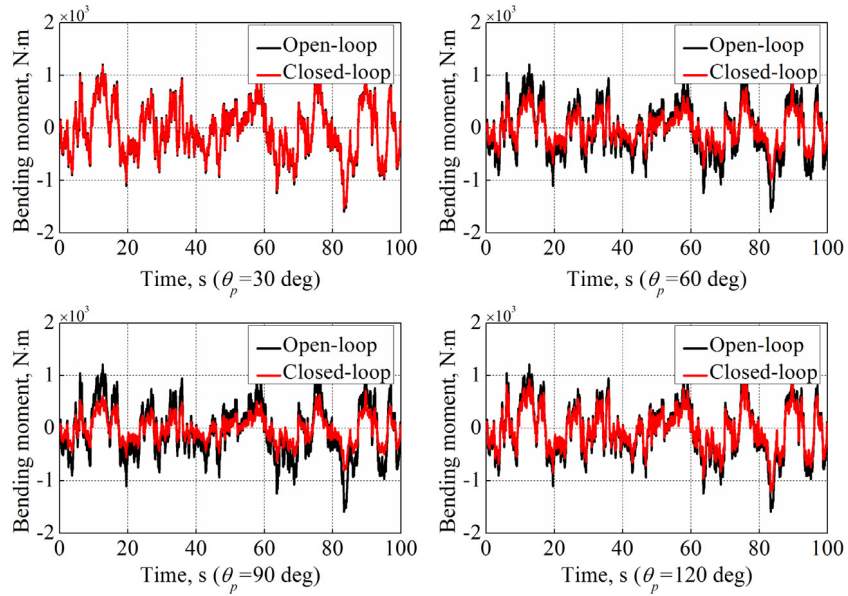
$$\begin{cases} \dot{\mathbf{x}}_g = \mathbf{A}_g \mathbf{x}_g + \mathbf{b}_g r \\ \tilde{\mathbf{w}}_g = \mathbf{C}_g \mathbf{x}_g \end{cases} \quad (29)$$

where the information of the matrices  $\mathbf{A}_g$ ,  $\mathbf{b}_g$  and  $\mathbf{C}_g$  is given in the [Appendix](#). By substituting Eq. (29) into Eq. (25), the state-space formulation of the open-loop aeroservoelastic equation can be obtained as

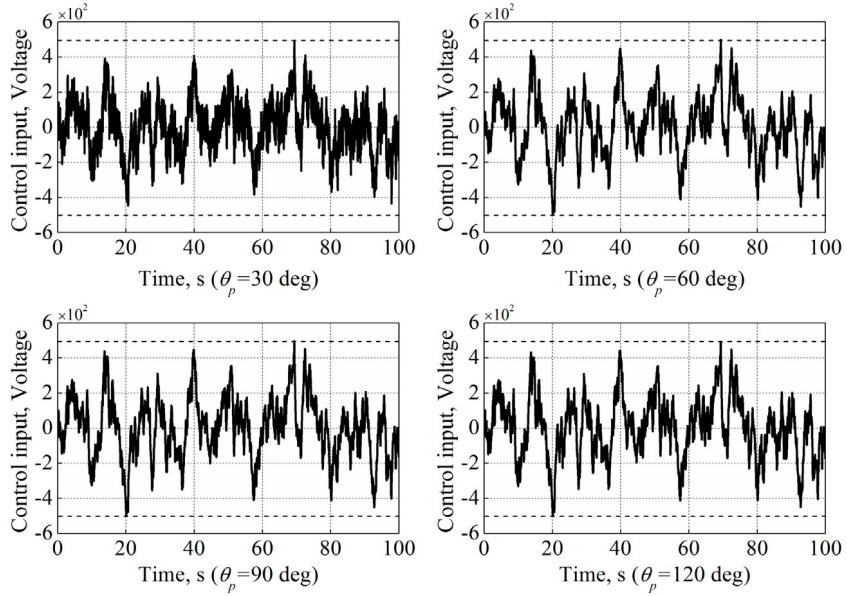
$$\dot{\mathbf{x}}_{ase} = \mathbf{A}_{ase} \mathbf{x}_{ase} + \mathbf{b}_{ase} V_p + \mathbf{b}_r r \quad (30)$$

where

$$\mathbf{A}_{ase} = \begin{bmatrix} \mathbf{A}_{ae} & \mathbf{B}_{aw} \mathbf{C}_g \\ \mathbf{0} & \mathbf{A}_g \end{bmatrix}, \quad \mathbf{x}_{ase} = \begin{bmatrix} \mathbf{x}_{ae} \\ \mathbf{x}_g \end{bmatrix}, \quad \mathbf{b}_{ase} = \begin{bmatrix} \mathbf{b}_p \\ \mathbf{0} \end{bmatrix}, \quad \mathbf{b}_r = \begin{bmatrix} \mathbf{0} \\ \mathbf{b}_g \end{bmatrix} \quad (31)$$



a) Time responses of the wing-root bending moment



b) Time responses of control input

**Fig. 10.** Dynamic responses of piezo-composite wings for case 2.

### 3. Aeroviscoelastic design for gust load alleviation

There are many design parameters which can influence gust load alleviation performance of the piezo-composite wing. For the simplicity, we will focus on the host structure configuration which has the maximum instability speed and investigate the effects of piezo-actuator ply-angle  $\theta_p$ . The geometric information of the piezo-composite wing under consideration is shown in [Table 1](#) and the material properties are shown in [Table 2](#).

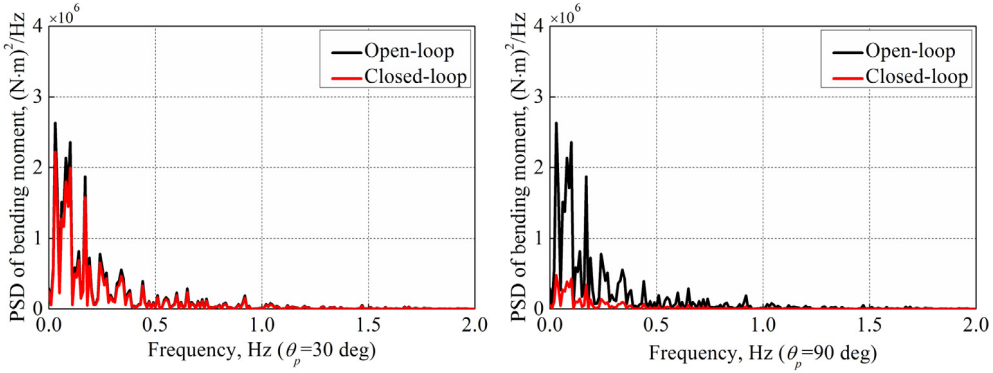


**Fig. 11.** PSD curves of the wing-root bending moment for case 2.

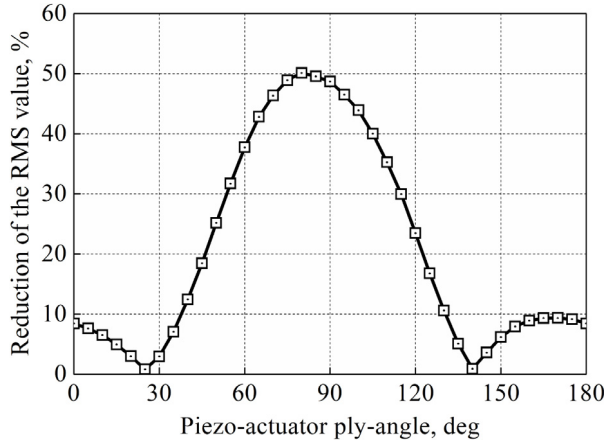


**Fig. 12.** Load alleviation performance of different piezo-composite wings for case 2.

### 3.1. Determination of the host structure configuration

In this subsection, the host structure configuration of the piezo-composite wing with maximum instability speed is determined by using the aeroservoelastic model shown in Eq. (30).

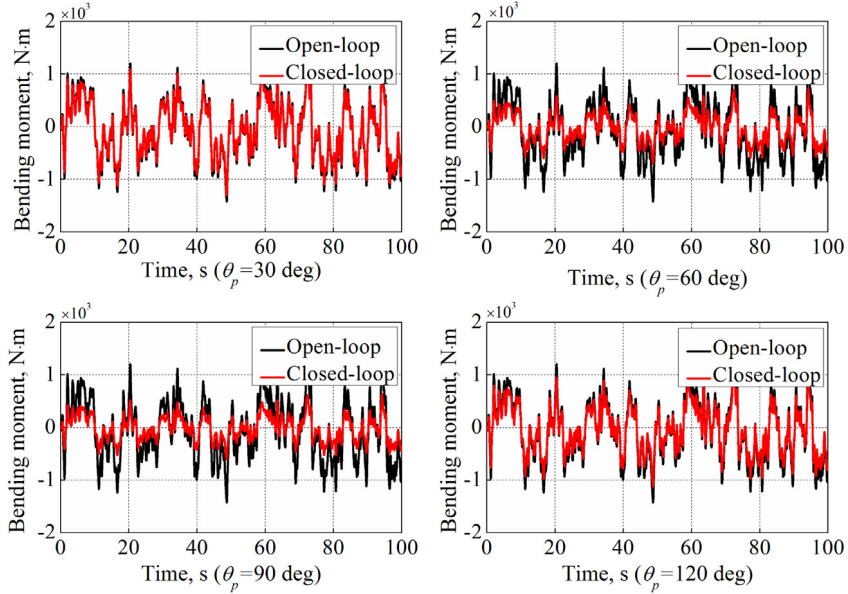
The aeroservoelastic modeling approach shown in Section 2 should be validated at first. Considering that the piezo-actuator part has been validated in Ref. Wang et al. (2017b), the aerodynamic model is specifically validated here. The flutter boundary of the composite wing developed by Qin and Librescu (2003) is investigated. Fig. 3 presents the aerodynamic grid used for the flutter boundary calculation. Fig. 4 presents the root-locus diagram of the composite wing. As shown in Fig. 4, the flutter speed of the composite wing is 146.2 m/s which is close to 139 m/s in Ref. Qin and Librescu (2003). Hence, the accuracy of the numerical modeling approach can be validated.

After performing extensive numerical simulations, it is found that six structural modes and four aerodynamic states are sufficient for the piezo-composite wing. In order to determine the host structure configuration with maximum instability speed, the static divergence speeds and flutter speeds are evaluated for host structure ply-angles  $\theta_h$  from 0 to 180 deg. Fig. 5 presents the variation trend of static divergence and flutter speeds.

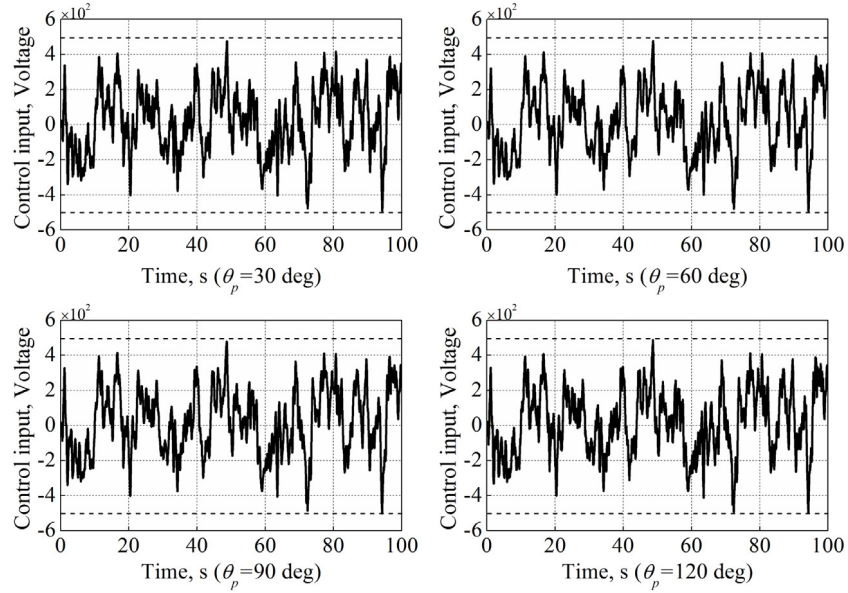
As shown in Fig. 5, when the host structure ply-angle  $\theta_h$  is between 0 and 90 deg, static divergence speed of the wing is small because of the negative elastic bending-twist coupling. On the contrary, higher static divergence speed is presented due to the strong positive elastic bending-twist coupling when the host structure ply-angle  $\theta_h$  is between 90 and 180 deg. In addition, it can be identified that adequate positive bending-twist elastic coupling is benefit for the improvement of the lowest flutter speed. It can be found the host structure ply-angle  $\theta_h = 130$  deg can produce the maximum flutter speed. We will focus on the piezo-composite wing with such host structure configuration in the remainder of this study.

### 4. Active aeroelastic control for gust loads alleviation

In this subsection, aeroservoelastic design to alleviate the continuous gust response is performed for the piezo-composite wing with host structure ply-angle  $\theta_h = 130$  deg. The influences of piezo-actuator ply-angles on gust load



a) Time responses of the wing-root bending moment



b) Time responses of control input

**Fig. 13.** Dynamic responses of piezo-composite wings for case 3.

alleviation performance are investigated. In order to produce maximum piezoelectrically induced actuations, the piezo-actuator is assumed spread over the entire wing span and is bounded outside the host structure. The material properties of the piezo-actuator is given in Table 2.

It is assumed that all state variables of Eq. (30), including the aeroelastic state  $\mathbf{x}_{ae}$  and the gust state  $\mathbf{x}_g$ , are available for feedback control. These state variables can be constructed by using a state estimator, which is out of the scope of the present work. Based on the aeroservoelastic model shown in Eq. (30), state feedback  $H_\infty$  controller can be synthesized for gust load alleviation according to robust control theory (Zhou and Doyle, 1998). Fig. 6 shows the  $H_\infty$  control diagram where  $M_r$  is the wing-root bending moment obtained via the mode displacement approach (Karpel et al., 2004). The

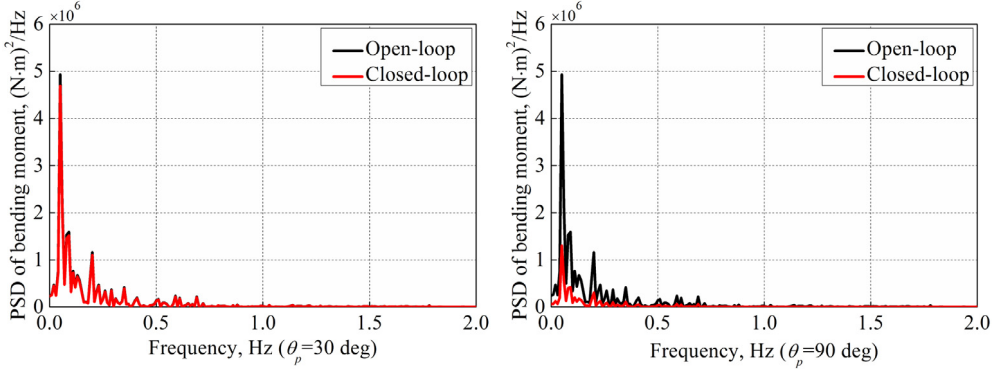


**Fig. 14.** PSD curves of the wing-root bending moment for case 3.

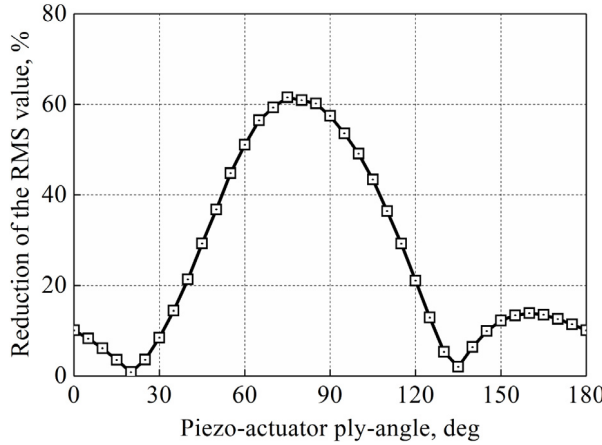


**Fig. 15.** Load alleviation performance of different piezo-composite wings for case 3.

term  $\eta$  represents the weight parameter that is used to adjust the conflicting design requirements. State feedback  $H_\infty$  controllers are synthesized for different piezo-composite wings under the same control input constraint, for which the range is  $-500 \text{ V} \sim 500 \text{ V}$ .

The gust load alleviation performance of piezo-composite wings with different piezo-actuator ply-angles is investigated for three flight conditions: Case 1–3. The corresponding flight parameters which include air speed  $V_\infty$ , density  $\rho_\infty$ , continuous gust scale  $L_w$  and RMS value of gust velocity  $\sigma_w$  are given in Table 3. State feedback  $H_\infty$  controllers for gust load alleviation are synthesized and the weight parameters for each configuration under the three flight conditions are presented in Table 4.

For case 1, Fig. 7 demonstrates the gust load alleviation performance and corresponding control input when the piezo-actuator ply-angles  $\theta_p$  are 30, 60, 90 and 120 deg, respectively. Fig. 8 presents the PSD curves of the wing-root bending moment for open-loop and closed-loop aeroservoelastic models with piezo-actuator ply-angle  $\theta_p = 30$  and  $\theta_p = 90$  deg. As shown by these results, there is almost no load alleviation effect for  $\theta_p = 30$  deg. The wing-root bending moment can be effectively reduced with piezo-actuator ply-angle  $\theta_p = 90$  deg.

The RMS value of the wing-root bending moment is evaluated for each wing configuration. Fig. 9 presents the reduction variation of the RMS value with piezo-actuator ply-angle. As shown in Fig. 9, the best load alleviation performance is obtained with the piezo-actuator ply-angle  $\theta_p$  around 80 deg. There is almost no load alleviation effect when the piezo-actuator ply-angle  $\theta_p$  is 25 or 140 deg.

For case 2, Fig. 10 presents the gust load alleviation performance and corresponding control input for the piezo-composite wing when the piezo-actuator ply-angles  $\theta_p$  are 30, 60, 90 and 120 deg, respectively. Fig. 11 presents the PSD curves of the wing-root bending moment for open-loop and closed-loop aeroservoelastic models with piezo-actuator ply-angle  $\theta_p = 30$  and  $\theta_p = 90$  deg. The RMS value of the wing-root bending moment is evaluated for each wing configuration. Fig. 12 presents the reduction variation of the RMS value with piezo-actuator ply-angle. As shown by these results, similar conclusions can be obtained as those of case 1. The best load alleviation performance is obtained with the piezo-actuator ply-angle  $\theta_p$  around 80 deg. This implies that piezoelectrically induced bending dominated active control in conjunction with adequate piezoelectrically induced twist is the optimal choice for gust load alleviation.

In order to further investigate the load alleviation performance for different flight condition, numerical simulations are performed for case 3. Fig. 13 demonstrates the gust load alleviation performance and corresponding control input for the piezo-composite wing when the piezo-actuator ply-angles  $\theta_p$  are 30, 60, 90 and 120 deg, respectively. Fig. 14 presents the PSD curves of the wing-root bending moment for open-loop and closed-loop aeroservoelastic models with piezo-actuator ply-angle  $\theta_p = 30$  and  $\theta_p = 90$  deg. Fig. 15 presents the reduction variation of the RMS value of wing-root bending moment with piezo-actuator ply-angle.

All these numerical results of case 1–3 demonstrate that the gust load alleviation performance is sensitive to the piezo-actuator ply-angle. There is an optimal configuration for gust load alleviation when the piezo-actuator ply-angle is around 80 deg. The load alleviation effect is immaterial when the piezo-actuator ply-angle is 25 or 140 deg.

## 5. Conclusions

In this study, the aeroservoelastic modeling approach of an adaptive piezo-composite wing is presented by integrating composite beam theory, doublet-lattice method and rational function approximation technique. The refined composite beam theory is a thin-walled beam theory which incorporating fiber-reinforced and piezo-composite layers. The anisotropic characteristics of piezo-actuators, which are usually neglected for aeroservoelastic modeling, are taken into account. The effects of piezo-actuator ply-angles on gust load alleviation performance are investigated and main conclusions are given as follows.

- (1) Significant load alleviation performance can be obtained for the piezo-composite wing by selecting appropriate piezo-actuator ply-angle.
- (2) Active control via piezoelectrically induced bending and twist coupling shows better performance on gust load alleviation than that of the pure piezoelectrically induced bending does.

## Acknowledgment

This work was supported by the National Natural Science Foundation of China under grant 11802120.

## Appendix

The matrices  $\mathbf{A}_{ae}$ ,  $\mathbf{b}_p$  and  $\mathbf{B}_{aw}$  read

$$\mathbf{A}_{ae} = \begin{bmatrix} \mathbf{0} & \mathbf{I} & \mathbf{0} \\ -\bar{\mathbf{M}}^{-1} (\mathbf{K} - q_\infty \mathbf{A}_{q0}) & -\bar{\mathbf{M}}^{-1} \left( \mathbf{D} - q_\infty \frac{b_R}{V_\infty} \mathbf{A}_{q1} \right) & q_\infty \bar{\mathbf{M}}^{-1} \mathbf{D}_w \\ \mathbf{0} & \mathbf{E}_q & \frac{V_\infty}{b_R} \mathbf{R}_w \end{bmatrix},$$

$$\mathbf{b}_p = [\mathbf{0} \ \bar{\mathbf{M}}^{-1} \mathbf{f}_p \ \mathbf{0}]^T,$$

$$\mathbf{B}_{aw} = \begin{bmatrix} \mathbf{0} & \mathbf{0} \\ \frac{q_\infty}{V_\infty} \bar{\mathbf{M}}^{-1} \mathbf{A}_{g0} & \frac{q_\infty b_R}{V_\infty^2} \bar{\mathbf{M}}^{-1} \mathbf{A}_{g1} \\ \mathbf{0} & \frac{1}{V_\infty} \mathbf{E}_g \end{bmatrix}$$

where

$$\bar{\mathbf{M}} = \mathbf{M} - q_\infty \left( \frac{b_R}{V_\infty} \right)^2 \mathbf{A}_{q2}$$

The matrices  $\mathbf{A}_g$ ,  $\mathbf{b}_g$  and  $\mathbf{C}_g$  read

$$\mathbf{A}_g = \begin{bmatrix} 0 & 1 & 0 \\ -\tau_w^{-2} & -2/\tau_w & a \\ 0 & 0 & -a \end{bmatrix}, \quad \mathbf{b}_g = \begin{bmatrix} 0 \\ 0 \\ \sigma_w/\sqrt{\pi} \end{bmatrix},$$

$$\mathbf{C}_g = \begin{bmatrix} \tau_w^{-3/2} & \sqrt{3}\tau_w^{-1/2} & 0 \\ -\sqrt{3}\tau_w^{-5/2} & (1-2\sqrt{3})\tau_w^{-3/2} & \sqrt{3}a\tau_w^{-1/2} \end{bmatrix}$$

## References

- Bae, J.S., Kyong, N.H., Seigler, T.M., et al., 2005. Aeroelastic considerations on shape control of an adaptive wing. *J. Intell. Mater. Syst. Struct.* 16 (11–12), 1051–1056.
- Barzegari, M.M., Dardel, M., Fathi, A., 2015. Control of aeroelastic characteristics of cantilever wing with smart materials using state-dependent Riccati equation method. *J. Intell. Mater. Syst. Struct.* 26 (8), 988–1005.
- Behal, A., Rao, V.M., Marzocca, P., et al., 2006. Adaptive control for a nonlinear wing section with multiple flaps. *J. Guid. Control Dyn.* 29 (3), 744–749.
- Candido de Sousa, V., De Marqui Jr., C., 2018. Experimental study on the aeroelastic behavior of a typical airfoil section with superelastic shape memory alloy springs. *J. Intell. Mater. Syst. Struct.* 29 (4), 623–635.
- Fang, D., Liu, J., 2013. Fracture Mechanics of Piezoelectric and Ferroelectric Solids. Springer, Heidelberg.
- Fonte, F., Ricci, S., Mantegazza, P., 2015. Gust load alleviation for a regional aircraft through a static output feedback. *J. Aircr.* 52 (5), 1559–1574.
- Giurgiutiu, V., 2000. Review of smart-materials actuation solutions for aeroelastic and vibration control. *J. Intell. Mater. Syst. Struct.* 11 (7), 525–544.
- Guo, S., 2007. Aeroelastic optimization of an aerobatic aircraft wing structure. *Aerosp. Sci. Technol.* 11 (5), 396–404.
- Haghhighat, S.T., Liu, H.H., RA Martins, J.R., 2012. Model-predictive gust load alleviation controller for a highly flexible aircraft. *J. Guid. Control Dyn.* 35 (6), 1751–1766.
- Han, J.H., Tani, J., Qiu, J., 2006. Active flutter suppression of a lifting surface using piezoelectric actuation and modern control theory. *J. Sound Vib.* 291 (3–5), 706–722.
- Heinze, S., Karpel, M., 2006. Analysis and wind tunnel testing of a piezoelectric tab for aeroelastic control applications. *J. Aircr.* 43 (6), 1799–1804.
- Huang, R., Hu, H., Zhao, Y., 2012a. Designing active flutter suppression for high-dimensional aeroelastic systems involving a control delay. *J. Fluids Struct.* 34, 33–50.
- Huang, R., Hu, H., Zhao, Y., 2012b. Single-input/single-output adaptive flutter suppression of a three-dimensional aeroelastic system. *J. Guid. Control Dyn.* 35 (2), 659–665.
- Huang, R., Qian, W., Hu, H., et al., 2015. Design of active flutter suppression and wind-tunnel tests of a wing model involving a control delay. *J. Fluids Struct.* 55, 409–427.
- Huang, R., Zhao, Y., Hu, H., 2016. Wind-tunnel tests for active flutter control and closed-loop flutter identification. *AIAA J.* 54 (7), 2089–2099.
- Jutte, C., Stanford, B.K., 2014. Aeroelastic Tailoring of Transport Aircraft Wings: State-of-the-Art and Potential Enabling Technologies.
- Kameyama, M., Fukunaga, H., 2007. Optimum design of composite plate wings for aeroelastic characteristics using lamination parameters. *Comput. Struct.* 85 (3–4), 213–224.
- Karpel, M., Moulin, B., Anguita, L., et al., 2004. Aeroviscoelastic gust response analysis for the design of transport aircrafts. In: AIAA-2004-1592.
- Kim, T.U., Hwang, I.H., 2005. Optimal design of composite wing subjected to gust loads. *Comput. Struct.* 83 (19–20), 1546–1554.
- Librescu, L., Khdeir, A., 1988. Aeroelastic divergence of swept-forward composite wings including warping restraint effect. *AIAA J.* 26 (11), 1373–1377.
- Librescu, L., Meirovitch, L., Na, S.S., 1997. Control of cantilever vibration via structural tailoring and adaptive materials. *AIAA J.* 35 (8), 1309–1315.
- Librescu, L., Meirovitch, L., Song, O., 1996. Refined structural modeling for enhancing vibrational and aeroelastic characteristics of composite aircraft wings. *Rech. Aerosp.* (1), 23–35.
- Librescu, L., Na, S., Qin, Z., et al., 2008. Active aeroelastic control of aircraft composite wings impacted by explosive blasts. *J. Sound Vib.* 318 (1–2), 74–92.
- Librescu, L., Song, O., 1991. Behavior of thin-walled beams made of advanced composite materials and incorporating non-classical effects. *Appl. Mech. Rev.* 44 (11S), S174–S180.
- Liu, H., Zhao, Y., Hu, H., 2016. Adaptive flutter suppression for a fighter wing via recurrent neural networks over a wide transonic range. *Int. J. Aerosp. Eng.* 2016.
- Livne, E., 2017. Aircraft active flutter suppression: State of the art and technology maturation needs. *J. Aircr.* 55 (1), 410–452.
- Lottati, I., 1985. Flutter and divergence aeroelastic characteristics for composite forward swept cantilevered wing. *J. Aircr.* 22 (11), 1001–1007.
- Mukhopadhyay, V., 2000. Transonic flutter suppression control law design and wind-tunnel test results. *J. Guid. Control Dyn.* 23 (5), 930–937.
- Na, S., Librescu, L., 1998. Oscillation control of cantilevers via smart materials technology and optimal feedback control: actuator location and power consumption issues. *Smart Mater. Struct.* 7 (6), 833.
- Na, S., Song, J.S., Choo, J.H., et al., 2011. Dynamic aeroelastic response and active control of composite thin-walled beam structures in compressible flow. *J. Sound Vib.* 330 (21), 4998–5013.
- Pettit, C.L., Grandhi, R.V., 2003. Optimization of a wing structure for gust response and aileron effectiveness. *J. Aircr.* 40 (6), 1185–1191.
- Qin, Z., Librescu, L., 2002. On a shear-deformable theory of anisotropic thin-walled beams: further contribution and validations. *Compos. Struct.* 56 (4), 345–358.
- Qin, Z., Librescu, L., 2003. Dynamic aeroelastic response of aircraft wings modeled as anisotropic thin-walled beams. *J. Aircr.* 40 (3), 532–543.
- Shirk, M.H., Hertz, T.J., Weisshaar, T.A., 1986. Aeroelastic tailoring-theory, practice, and promise. *J. Aircr.* 23 (1), 6–18.
- Suleiman, A., Costa, A.P., 2004. Adaptive control of an aeroelastic flight vehicle using piezoelectric actuators. *Comput. Struct.* 82 (17–19), 1303–1314.
- Wang, X., Morandini, M., Maserati, P., 2017a. Modeling and control for rotating pretwisted thin-walled beams with piezo-composite. *Compos. Struct.* 180, 647–663.
- Wang, X., Morandini, M., Maserati, P., 2017b. Velocity feedback damping of piezo-actuated wings. *Compos. Struct.* 174, 221–232.
- Wang, X., Qin, Z., 2016. Nonlinear modal interactions in composite thin-walled beam structures with simultaneous 1: 2 internal and 1: 1 external resonances. *Nonlinear Dynam.* 86 (2), 1381–1405.
- Wang, X., Zhou, W., Wu, Z., 2018. Feedback tracking control for dynamic morphing of piezocomposite actuated flexible wings. *J. Sound Vib.* 416, 17–28.
- Weisshaar, T.A., Duke, D.K., 2006. Induced drag reduction using aeroelastic tailoring with adaptive control surfaces. *J. Aircr.* 43 (1), 157–164.
- Yang, J., 2004. An Introduction to the Theory of Piezoelectricity, Vol. 9. Springer Science & Business Media.
- Zeng, J., Kukreja, S., Moulin, B., 2012. Experimental model-based aeroelastic control for flutter suppression and gust-load alleviation. *J. Guid. Control Dyn.* 35 (5), 1377–1390.
- Zhang, R., Singh, S.N., 2001. Adaptive output feedback control of an aeroelastic system with unstructured uncertainties. *J. Guid. Control Dyn.* 24 (3), 502–509.
- Zhao, Y., Yue, C., Hu, H., 2016. Gust load alleviation on a large transport airplane. *J. Aircr.* 53 (6), 1932–1946.
- Zhou, K., Doyle, J.C., 1998. Essentials of Robust Control. Prentice hall, Upper Saddle River, NJ.